DOI: 10.13009/EUCASS2023-688
Aerospace Europe Conference 2023 – 10TH EUCASS – 9TH CEAS

Investigating the power and energy flows for a Kinetic Energy Recovery System from a landing aircraft

Andre MANICOLO[1], Cedric CARUANA[2] and Robert CAMILLERI[3]*

** Corresponding author*

[1] Institute of Aerospace Technologies, University of Malta, Malta, andre.manicolo@um.edu.mt
[2] Dept. Ind. Electrical Power Conv., University of Malta, Malta, cedric.caruana@um.edu.mt
[3]Institute of Aerospace Technologies, University of Malta, Malta, robert.c.camilleri@um.edu.mt

Abstract

This paper investigates the power and energy flows for a kinetic energy recovery system from a landing aircraft. The concept studied here uses electrical motors installed at the wheels to produce regenerative braking during rollout. This energy is stored temporarily into a flywheel energy storage device and is then transferred back to the wheels for engineless taxiing. The paper develops an aircraft dynamics model to assess the bi-directional power and energy transfer. The model is tested with two case studies; the A320 and the ATR-72 aircraft, thus assessing a wide spectrum for short haul flights. Simulated results show that during normal operation, there is sufficient energy that can be harvested from a landing aircraft that may be used for taxiing purposes. However, the short rollout time places a stringent demand on the system which is limited by the safety aspect of performance limited runways or busy major airports requiring minimum runway occupancy time operation. This limitation can be overcome by increasing the motor torque rating.

1. Introduction

As part of the efforts towards the abatement of climate change, the European Union (EU) has set aggressive targets for the reduction of emissions from air travel. While in the last decade, R&D targeted the airborne phase, the EU is now legislating so that all aircraft movements on the ground will be emission-free by 2050 [1]. Airport carbon footprint analysis and accreditation demonstrate that aircraft ground movement accounts between 5-20% of all airport emissions [2]. Conventionally, engine thrust is used during taxiing to provide forward propulsion. A typical 10-minute taxiing process for a narrow body aircraft consumes approximately 100 kg of fuel with a considerable amount of carbon and NOx pollutants released at ground level. The reduction of emissions on the ground is important as it has strong links with respiratory illnesses, amongst others. As airports and cities continue to grow, these get in closer proximity to each other, heightening the effects of the problem.

The environmental impact of the various taxiing techniques with reference to the baseline standard taxiing method was studied [3]. It was shown that onboard technologies have lower taxiing emissions than the use of tow trucks. The latter can only be truly effective if electric trucks are used and the energy used to charge their batteries is provided by a high percentage of renewables with low emission index. Onboard solutions offer fewer logistical challenges to implement and allow aircraft to maintain their autonomy in airport operations. This characteristic is preferred by airlines which are keen to remove dependencies. However, studies on electrical taxiing showed that while motor technology was viable, the auxiliary power unit (APU) had to be redesigned such that the generator would be able to supply sufficient electrical power to the in-wheel motors [4]. This would result in a costly retrofit. This paper addresses this shortcoming and proposes that a portion of the kinetic energy of the aircraft is recovered during the landing rollout. The concept studied here uses electrical motors installed at the wheels to produce regenerative braking during landing. This energy is stored temporarily into a flywheel energy storage device and is then transferred back to the wheels for engineless taxiing. A flywheel energy storage system (FESS) was selected due to its high-power density and high energy density characteristics. A schematic of the system components and the energy flow between them is shown in Figure 1. In our work, we consider a slow-speed, high torque traction motor (TMs) installed at each wheel of the main landing gear (MLG). The TMs are mechanically coupled to the wheels and electrically coupled via a power electronic converter to a high-speed flywheel machine, which in turn is mechanically coupled to a composite flywheel.

The study presented here investigates the power flows that happen whilst charging and discharging the flywheel. The paper is therefore organised in the following manner. Section 2 provides an overview of the aircraft dynamics during landing and taxiing, with the respective forces acting on the system components. Section 3 presents the model developed to establish the bidirectional energy and power flows. The model is applied to two case studies: A short

DOI: 10.13009/EUCASS2023-688

haul, single aisle aircraft A320 and a regional aircraft ATR72. The case studies and the respective aircraft parameters are presented in Section 4. The results are presented in Section 5 and finally a discussion and conclusion are presented in Section 6.

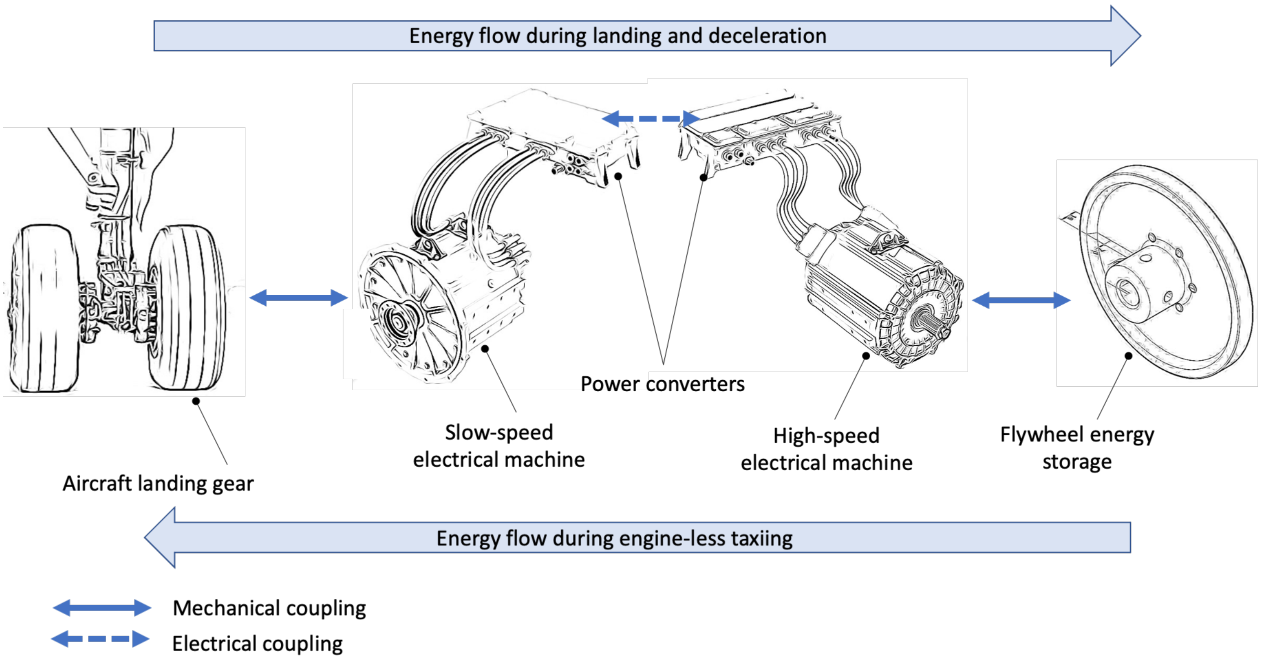

Figure 1: Schematic showing the main parts of the system and the direction of the energy flow.

2. Aircraft Dynamics Theory

Having described the overall system, this section describes the aircraft dynamics theory and the forces acting on the aircraft during taxiing as shown in Figure 2.

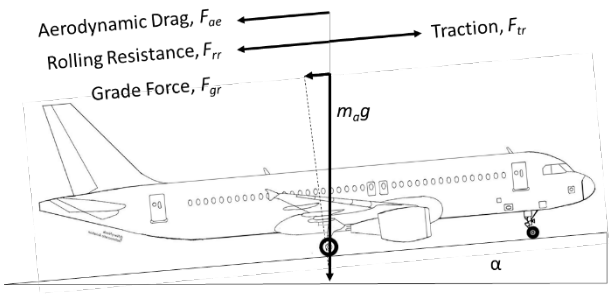

Figure 2: Forces acting on an aircraft on the ground during taxi

The dynamics model considers the longitudinal forces acting on the aircraft during ground movement. The forces combine to form the traction force F_{tr} driving the aircraft and the opposing force F_o. The difference between the two forces yields the linear acceleration, as expressed in (1) where m_a is the mass of the aircraft, and $\frac{dv}{dt}$ the linear acceleration.

$$F_{tr} - F_o = m_a \frac{dv}{dt} \tag{1}$$

The opposing force F_o is composed of three main components, mainly the rolling resistance F_{rr}, the aerodynamic resistance F_{ae} and the gradient resistance F_{gr} as in (2).

$$F_o = F_{rr} + F_{ae} + F_{gr} \tag{2}$$

The rolling resistance represents the hysteresis losses in the tires. It is characterised by the μ_{rr} coefficient as shown in (3), where g is the gravitational constant while α is the taxiway slope.

DOI: 10.13009/EUCASS2023-688

$$F_{rr} = \mu_{rr} m_a g cos(\alpha) \tag{3}$$

The aerodynamic resistance F_{ae} is the drag produced by the aircraft. It is determined by the drag equation (4), where ρ is the density of the air, A_{wing} is the equivalent wing area, C_D is the aircraft drag polar coefficient and v is the linear velocity of the aircraft.

$$F_{ae} = \frac{1}{2}\rho A_{wing} C_D v^2 \tag{4}$$

The taxiway slope presents an additional component to the opposing forces, and this is represented by (5).

$$F_{gr} = m_a g sin(\alpha) \tag{5}$$

2.1 Landing Roll Forces

A typical medium haul aircraft uses multiple techniques to aid the deceleration during the landing roll. These include, ground spoilers on top of the wings to add drag, reverse thrust that directs the engine thrust backwards and disc braking on the MLG. During the landing roll these braking forces combine together with the opposing forces and the traction force produced by the motors (acting in the opposing direction) to create a deceleration force. Since α is typically $\simeq 0$, all braking forces are assumed to act in the horizontal plane. The spoiler drag F_{sp} is determined by the drag formula (6), where A_{sp} is the frontal area of the spoilers, and C_{SP} is the coefficient of drag (CoD) for a rectangular plate in an airflow. The frontal area, A_{sp}, of the spoilers is determined by (7) where n_{sp} is the number of spoilers, L is the length of one spoiler, b is the width, and θ_{max} is the deflection of the spoilers during landing. According to Mahmood et al [5], the total reverse thrust produced by the aircraft engines F_{rt} is proportional to the forward velocity of the aircraft. The variation is quite linear with a low gradient, so the thrust was taken as constant, k_{rt} (8), throughout the landing roll. The reverse thrust is on until deselected by the pilot when the aircraft speed drops to 70 knots (aircraft limitation).

$$F_{sp} = \frac{1}{2}\rho A_{sp} C_{SP} v^2 \tag{6}$$

$$A_{sp} = n_{sp} L b \sin(\theta_{max}) \tag{7}$$

$$F_{rt} \simeq k_{rt} \tag{8}$$

The braking force produced by the MLG brakes F_{br}, depends on how the brakes are applied during the rollout. The brakes can be commanded by the pilot by exerting pressure on the brake pedal, or in the case of a typical medium haul aircraft, through the autobrake function based on the set deceleration value. For this study, the autobrake function is used. The force F_{br} is added onto the TM force to achieve the set deceleration.

2.2 Flywheel Energy Storage

The power flow in the flywheel for charging and discharging operation is shown in (9) and (10) respectively. The efficiency η_{pc} represents the power losses in the power converter while η_{em} accounts for the losses in the electrical machines. The number of TMs in the system is defined by n_{TM}, the torque per TM by τ_{TM}, and the angular rotation of the TMs by ω_{TM}. The resulting flywheel motor torque is given by (11), where τ_{FW} is the flywheel motor torque and ω_{FW} is the angular rotation of the flywheel motor.

$$P_{FW}^{chg} = -\eta_{pc}\eta_{em} n_{TM} \tau_{TM} \omega_{TM} \tag{9}$$

$$P_{FW}^{dcg} = -\frac{1}{\eta_{pc}}\frac{1}{\eta_{em}} n_{TM} \tau_{TM} \omega_{TM} \tag{10}$$

$$\tau_{FW} = \frac{P_{FW}}{\omega_{FW}} \tag{11}$$

Neglecting friction, the flywheel dynamic equation is shown in (12), where J_{FW} is the moment of inertia of the flywheel. The energy stored in the flywheel can be represented by (13).

DOI: 10.13009/EUCASS2023-688

$$J_{FW}\frac{d\omega_{FW}}{dt} = \tau_{FW} \tag{12}$$

$$E_{FW} = \frac{1}{2}J_{FW}{\omega_{FW}}^2 \tag{13}$$

3. Software Modelling

A software model was designed and implemented in MATLAB Simulink. It is comprised of five blocks, where the Rollout and Taxi blocks drive the Aircraft dynamics block. The output of the latter block then allows calculation of the power transfer with the flywheel and subsequently the energy stored. A schematic diagram of the software model is shown in Figure 3. The following sub sections describe the individual blocks of the model.

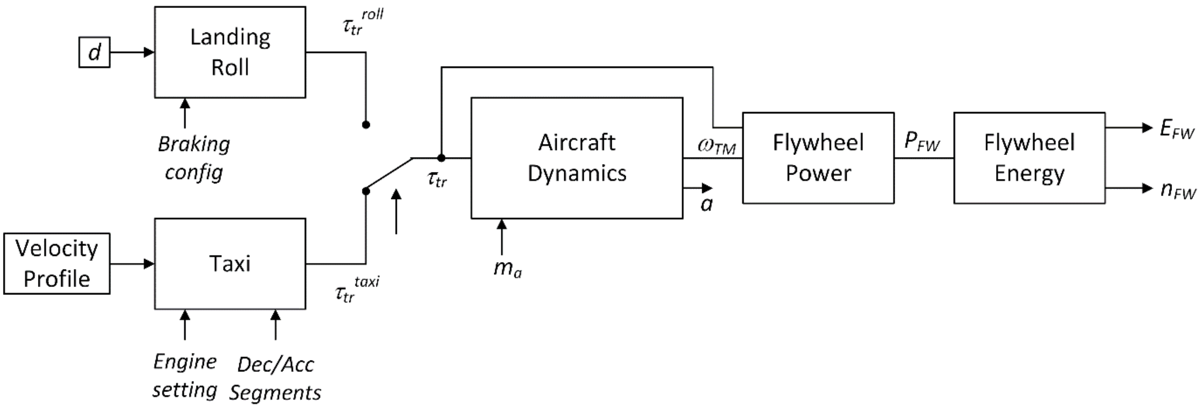

Figure 3: Schematic diagram of the software model

3.1 Aircraft Dynamics Block

The Aircraft Dynamics block implements the longitudinal dynamics described by (1) - (5). The block is expressed in terms of torque at the shaft of the TMs as in (14), where *r* is the radius of the MLG wheel.

$$n_{TM}J_{TM}\frac{d\omega_{TM}}{dt} = \tau_{tr} - r\left(F_o + m_a\frac{dv}{dt}\right) \tag{14}$$

Expressing the linear velocity *v* in terms of the rotational speed ω_{TM}, as expressed in (15), allows combining the TM inertia with the aircraft mass to obtain the total equivalent inertia J_T as shown in (16). The total equivalent inertia is expressed in (17), considering that $J_{TM} << J_T$.

$$v = r\omega_{TM} \tag{15}$$

$$\frac{d\omega_{TM}}{dt} = \frac{1}{J_T}(\tau_{tr} - rF_o) \tag{16}$$

$$J_T = n_{TM}J_{TM} + m_a r^2 \simeq m_a r^2 \tag{17}$$

The aircraft mass m_a is kept as an input variable to reflect the difference in fuel mass between taxi in and taxi out phases. The block outputs the rotational speed ω_{TM} and its derivative, from which the aircraft linear velocity *v* and acceleration *a* are calculated.

3.2 Landing Roll Block

The landing roll block is driven by a constant deceleration setting *d*, and allows setting of different braking configurations through the three component braking forces, i.e. engine reverse thrust, ground spoilers and wheel disc brakes. The reference deceleration *d* as demanded by the autobrake setting is compared to the actual deceleration from the Aircraft Dynamics block to determine the required TM and disc brake torques. The engine reverse thrust and ground spoilers' forces were expressed in (6) and (8). The resulting traction torque during roll operation is expressed in (18). The traction torque is positive when the TM is supplying traction force in the forward direction whereas it is negative when the TM is being used to provide a braking force during the landing roll.

DOI: 10.13009/EUCASS2023-688

$$\tau_{tr}^{roll} = n_{TM}\tau_{TM} - r\left(F_{rt} + F_{sp} + F_{br}\right) \tag{18}$$

The block is only operational during the first 30s of the simulation. This setting allowed adequate time for the aircraft to decelerate to a safe taxi speed after landing for the different scenarios which were simulated.

3.3 Taxi Block

The taxi block is driven by a velocity profile representing the taxi-in from runway vacation until stopping at the gate, a stationary period at the gate and a taxi out sequence to the take-off point.

The predefined taxi profile, as shown in the upper plot of Figure 5 (a), consists of a sequence made up of 5 minutes taxiing from the runway to the stand, 5 minutes stopped at the gate and 5 minutes taxiing out for a new flight. These average taxi time values were derived from historical values for different airports as published by Eurocontrol [6]. The turnaround at the gate is usually much longer than 5 minutes but this value was assumed in order to contain the simulation time and assuming that there are no significant changes in the flywheel energy during this time. An evolution of this profile was produced in order to study the effect of introducing a deceleration/acceleration segment during taxi, as can be seen in the upper plots of Figure 9 (a) and (b). The segments were introduced during the engine idle period or when the engines were shut down.

Aircraft engine manufacturers require a cooldown/warmup period after/before applying high engine thrust in order to achieve thermal stabilisation in the engine core. This requirement is considered in the taxi block, where the engine idle thrust is added onto the TM thrust for the required period. The idle thrust is assumed constant from taxi speed until engine shutdown after landing and from engine start until the takeoff point during taxi-out.

The taxi block determines the torque requirement from the TMs by comparing the actual aircraft speed to that set by the taxi profile. The block then outputs the total traction torque as expressed in (19), where F_{me}, is the thrust produced by the main engines. The torque generated by the TMs is positive when it is providing forward traction, whilst it is negative whenever it is providing braking. Priority is given to regenerative braking during the taxi profiles so the wheel brakes were not used. During the cooldown/warmup period, the main engine force, F_{me} will be constant equal to the idle thrust, k_{it} as shown in (20).

$$\tau_{tr}^{taxi} = n_{TM}\tau_{TM} + rF_{me} \tag{19}$$

$$F_{me} = k_{it} \tag{20}$$

The switchover between the landing roll block and the taxi block occurs when the aircraft speed reduces to a safe taxi speed threshold of 20 knots during the landing roll.

3.4 Flywheel Power and Energy Blocks

The flywheel power and energy blocks work out the power and energy flows that occur between the TMs and the flywheel motor according to equations (9) – (13). The flywheel power block is driven by the total TM torque $n_{TM}\tau_{TM}$ and the rotational speed to determine the power flow between the TMs and the flywheel. The block considers efficiency values for the electrical machines and the power convertor. The power flow for charging and discharging operation was presented in (9) and (10) respectively.

The flywheel energy blocks is driven by the power to determine the flywheel torque τ_{FW} as per (9) and (10). The block implements (12) and (13) to determine the flywheel rotational speed ω_{FW} and stored energy E_{FW} respectively. The minimum flywheel speed is limited to 10% of the rated value. When the speed reaches this limit, further discharge is disabled requiring the use of the main engines for completing the taxi profile.

4. Case Studies

Having discussed the model and its governing equations, this section turns its focus to its application to two case studies. Short haul flights are efficiently performed through regional jets and single-aisle, narrow body aircraft such as the Airbus A320 and Boeing 737 aircraft. In Europe and the US, low-cost carrier dominate the short haul market. Such airlines have a typical turnaround time of approximately 25 minutes, with each aircraft managing between 3-5 flights daily. This is important in our context as every aircraft in the fleet spends more time on the ground, and consumes over

DOI: 10.13009/EUCASS2023-688

1 tonne of fuel for taxiing operations per day. To enhance the return on investment on such a system and provide a unique opportunity to turn an existing emission problem into a green solution. This paper considers two narrow body aircraft, the Airbus A320 and the ATR-72, illustrated in Figure 4 respectively. These were strategically chosen to represent both ends of the spectrum of the narrow body aircraft class and to examine the scalability of the proposed system.

Figure 4: The A320 NEO (left) and ATR-72 (right) considered as case studies in this paper. Images from [7,8].

The Airbus A320 NEO is a popular twin jet aircraft capable of carrying up to 194 passengers with a maximum range of 6300km. It is one of the most commonly used aircraft in Europe and around the world for short haul and medium haul flights. It has a Maximum Take-Off Weight (MTOW) of 79 tonnes, depending on options. Conversely, the ATR-72 is a twin-engine turboprop aircraft that is primarily used for regional and short-haul flights. It is capable of carrying 72 passengers in a single aisle configuration with a maximum range of approximately 2800km and a MTOW up to 23 tonnes.

The landing gear of both aircraft is very similar and consists of two main gears positioned in the mid-section of the aircraft and a steerable nose gear that is located in the front section of the aircraft. Each MLG has two main wheels on a single hub and retracts inboard in the fuselage. The nosewheel also has two wheels that retract forward, beneath the nose section. Both aircraft are thus suitable contenders for the installation of TMs on the MLG.

The A320 has an autobrake system with three different settings that can be set by the pilot during the setup for landing depending on the landing performance required and the runway condition. LO and MED are the two settings that are used for landing. Ground spoilers located on the wings engage as soon as the aircraft touches the ground. The primary use for these spoilers is to dump lift from the wing and transfer the whole weight of the aircraft on the landing gear thus making wheel braking more effective. The spoiler panels create additional drag that aid in the deceleration process. The A320 has reverse thrust on the engines, achieved by blocker doors in the bypass section of the engine. When operated, airflow through the engine is directed to oppose the forward motion of the aircraft. These three mentioned features are not present on the ATR-72, mainly due to the lower energy requirement to decelerate the considerably lighter aircraft.

4.1 Aircraft Parameters

Table 1 presents the different parameter categories which were used in the model to create a realistic representation of the aircraft in question. The physical aircraft parameters category describes the dimensions, weight and the thrust produced by the engines at idle or at reverse for the A320. The aircraft settings category presents those parameters which are adjusted according to the operational requirement, depending on the aircraft weight and required performance. The coefficients category presents the coefficients used in the equations to determine the drag produced by the opposing force F_o and by the spoilers in the case of the A320. According to Sun et al [17], the difference in C_D for different types of aircraft is insignificant. Thus the CoDs for the opposing forces were assumed to be the same for both aircraft types since no reference was available for the ATR-72. The rolling resistance coefficient μ_{rr} is dependent on the tire pressure, which is a property of the tire. Thus this coefficient was assumed to remain constant for both aircraft. The physical constants in the last category are commonly used natural environmental constants.

In order to keep the simulation as accurate as possible, the mass of the aircraft m_a was changed according to the phase of the of the flight. It was considered as MLW for the landing rollout and for the taxi-in part, and MTOW for the taxi-out part. This is in order to cater for the difference in the fuel load. In scenario 2 a more practical weight was considered,

DOI: 10.13009/EUCASS2023-688

in which the landing weight was assumed at 59 tonnes, whereas the take-off weight was considered at 69t. Different approach speeds V_{land} were also considered to reflect the landing weight. C_D is dependent on the aircraft configuration so two different values were used to distinguish between the landing configuration and taxi configuration.

Table 1: Real aircraft parameters used in the software model

Parameter	A320 - NEO	ATR-72	Description
Physical Aircraft Parameters			
A_{wing} [m^2]	123.0 [9]	61.0 [10]	equivalent wing area
$MTOW$ [tonnes]	79.0 [7]	23.0 [8]	Maximum Take Off Weight
MLW [tonnes]	67.4 [7]	22.4 [8]	Maximum Landing Weight
r [m]	0.584 [11]	0.432 [12]	MLG tire radius
L [m]	1.6 [13]	n/a	average spoiler length
b [m]	0.625 [13]	n/a	average spoiler depth
θ_{max} [°]	50 [14]	n/a	maximum angle of deflection of spoiler
n_{sp}	10	n/a	number of spoilers
k_{it} [kN]	7.5 [11]	2.6 [15]	engine idle thrust
k_{rt} [kN]	75 [5]	n/a	total force produced by reverse thrust
Aircraft Settings			
T_{en} [s]	180	150	engine cooldown/warmup time
$V_{land\ (MLW)}$ [knots]	140	113	approach speed at MLW
$V_{land\ (59t)}$ [knots]	134	n/a	approach speed at 59 tonnes
d_{LO} [m/s^2]	2.0	n/a	autobrake deceleration setting (LO)
d_{MED} [m/s^2]	3.0	n/a	autobrake deceleration setting (MED)
Coefficients			
C_{SP}	1.5 [16]	n/a	CoD for spoiler
C_D (landing)	0.12 [17]		CoD for an aircraft in landing configuration
C_D (taxi)	0.055 [17]		CoD for an aircraft at taxi configuration.
μ_{rr}	0.009 [18]		rolling resistance coefficient
Physical Constants			
g [m/s^2]	9.81		gravitational constant
α [°]	0.5		runway/taxiway slope
ρ [kg/m^3]	1.225		density of air at mean sea level

4.2 System Parameters

This paper considers a base profile for taxi-in and -out operations following initial rollout, as shown in the upper part of Figure 5 (a). The initial rollout follows the set autobrake deceleration setting. As soon as the aircraft reaches the taxi speed v_{taxi} of 20 knots, the speed is maintained constant until the aircraft starts decelerating with a rate of 0.4m/s^2 to stop at the gate at the 5-minute mark. For taxi-out operation, a similar profile is used with an initial acceleration of 0.2m/s^2. Various options to the profile are introduced in the case studies where deceleration and acceleration segments are introduced as reported in Section 4.1.3. In order to maximise the taxi range capability, regenerative braking is given priority over the use of mechanical brakes. The torque rating of the TMs was thus set to allow reaching the deceleration and acceleration requirements solely through the TMs. Maximum torque requirements of 9.7kNm and 3.3kNm for the A320 and ATR-72 respectively were obtained. Using these torque ratings, the highest energy transfer to the flywheel was determined. The flywheel rating was set to a slightly higher value to allow for a 10% safety margin. In order to restrict the overall mass of the flywheel, a maximum rotational speed of 60krpm [19] was set. The flywheel inertias were then determined through (13). The set system parameters are summarised in Table 2.

DOI: 10.13009/EUCASS2023-688

Table 2: Table showing the proposed system parameters that were used in the model

Parameter	A320-NEO	ATR-72	Description
v_{taxi} [knots]	20		steady taxi speed
E_{max} [MJ]	50.0	17.5	maximum energy in FESS
n_{FW} [rpm]	60 000	60 000	maximum rotational speed of flywheel
J_{FW} [kg.m^2]	2.53	0.87	moment of inertia of the flywheel
τ_{max} [kNm]	9.7	3.3	maximum motor torque per MLG
n_{TM}	2		number of TMs
η_{pc}	0.95		efficiency of power converter
η_{em}	0.95		efficiency of electrical machines

5. Results

This section presents the results of four scenarios which were carried out, three for the A320 and one for the ATR-72. Each scenario compares two cases with different settings. The scenarios mainly compare the effects of using different deceleration aids to the energy recovered during landing and to the possible taxi time which can be achieved. Since the A320 has more deceleration aids than the ATR-72 during the landing roll, the majority of the studies were performed on the former type of aircraft. Selected configurations were then applied to the ATR-72, and the results show the outcomes which were achieved.

5.1 A320

The three main deceleration aids during landing for the A320 are; reverse thrust, spoilers and disc braking. The aircraft has two autobrake settings; LO and MED corresponding to the deceleration rates shown in Table 1. Simulations were performed and these parameters were systematically changed for two landing weights in order to study the effect on the proposed system. Ground spoiler use during landing is not usually optional, unless there is some failure, so in the tests performed it was assumed that the spoilers were always deployed. The first two scenarios presented below compare different deceleration aids and rates, mainly through reverse thrust and autobrake settings. The third scenario introduces deceleration/acceleration events in order to study the consequence of having a pause in the taxi procedure due to Air Traffic Control (ATC) exigencies.

5.1.1 Scenario 1 – Comparison between Idle Reverse and Full Reverse at MLW

The first scenario considers a fully laden A320 with different reverse thrust settings whilst maintaining a LO autobrake deceleration during rollout. Engine cooldown and warmup periods of 180s at the start of taxi-in and at the end of taxi-out phases are included. Operation with Idle and Full Reverse thrust settings is shown in Figure 5 (a) and (b) respectively. The top plot shows the actual aircraft speed, starting from rollout and followed by the three phases of the base taxi profile. The middle plot shows the energy stored in the flywheel. The bottom plot shows the various interacting force components expressed as equivalent torques on the shaft of the TMs.

The aircraft speed starts from the landing speed of 140 knots (see Table 1) and drops linearly according to LO autobrake deceleration setting. In order to visualise the multiple contributions to the landing roll braking, the first 40s of the torque plots for idle and full reverse thrust settings are shown in Figure 6 (a) and (b) respectively. For the idle thrust case, initially, the main deceleration is achieved by the contribution of the opposing force F_o, the spoiler drag and TM torque. The brake force fills in to maintain a constant total torque as required by the deceleration setting. As the aircraft decelerates, the drag produced by F_o and the spoilers drops thus more braking is required. The TM torque is seen to start contributing to the deceleration immediately, where it reaches and maintains its maximum value and thus extracting maximum energy for charging the flywheel.

In the full reverse thrust case, the reverse thrust acts in addition to the previous torques. It can be seen that the former is significant and is the main contributor during its deployment. During the initial part, the total torque trace shows that more than the required deceleration is being achieved through these conventional methods, leaving no space for the TMs to operate. Thus, both the brakes and the TMs are not active in this period. As the force F_o and the spoiler drag reduce with aircraft speed, the TM torque rises hence starting the power transfer to the flywheel (at around 8s). The reverse thrust is set to idle by the pilot when the aircraft speed drops to 70 knots, at which point the TM torque picks

DOI: 10.13009/EUCASS2023-688

up and reaches the maximum value. The maximum TM torque is however not enough to maintain the required deceleration, so the model starts applying the aircraft brakes to provide the rest of the torque needed to achieve the set deceleration.

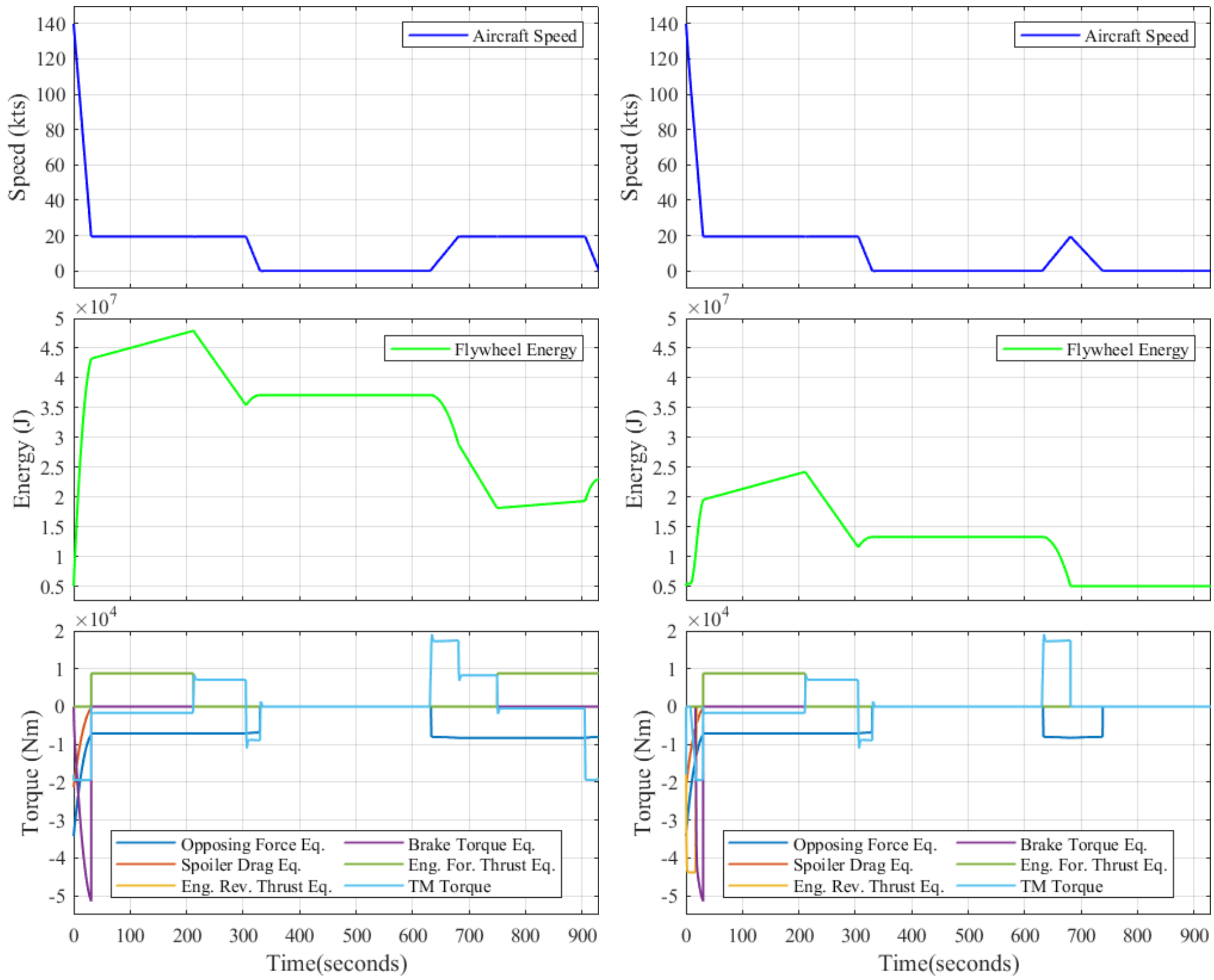

(a) (b)

Figure 5: Aircraft Speed, Flywheel Energy and Equivalent Torques for the A320 using (a) Idle and (b) Full reverse thrust setting during rollout. Aircraft weight is at MLW, LO Autobrake setting.

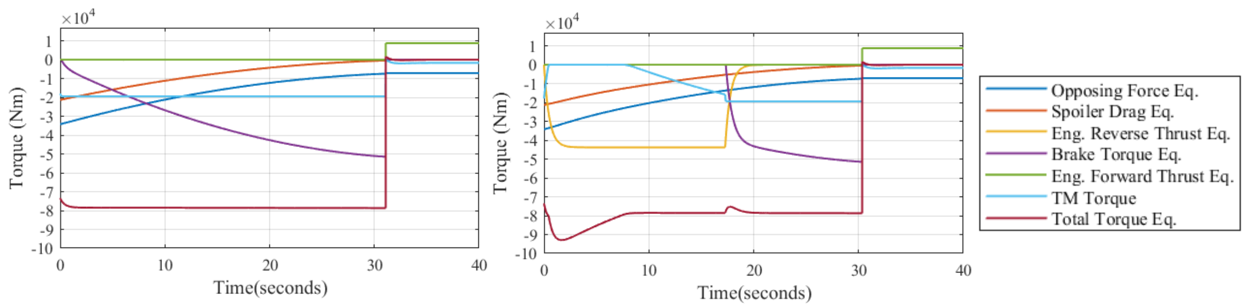

(a) (b)

Figure 6: Deceleration torques acting during the landing roll with (a) idle and (b) full reverse thrust. The plots correspond to the first 40s of the lower plots on Figure 5.

The rollout period is crucial for the charging of the FESS. The later use of maximum TM torque for operation with reverse thrust implies less energy transfer to the FESS. The flywheel energy plots in Figure 5 show corresponding values of 43.3MJ and 19.4MJ respectively, implying a reduction of around 55% of initial energy capture due to the use of full reverse thrust. In both cases, there is scope for higher TM torque rating for higher power transfers to the FESS. The torque rating is limited from considerations of the maximum mass of the proposed system.

DOI: 10.13009/EUCASS2023-688

In both cases, as soon as the aircraft reaches the taxi speed of 20 knots, the pilot deselects idle reverse and in consequence the engine idle thrust comes on. This thrust contributes to the traction force F_{tr} to follow the initial part of the taxi profile. The case of the A320 NEO is considered [11], where the idle thrust exceeds the required F_{tr} for the considered scenario. Consequently, as can be seem from the lower plot in Figure 5 (a), the TM torque τ_{TM} continues to provide a slight opposing force during taxi whenever the engines are at idle, hence leading to further charging of the FESS. The charging is confirmed by the positive slope in the flywheel energy shown by the middle plot. The respective flywheel energies reach values of 47.8MJ and 24.2MJ respectively, i.e., an increase of 10% for the idle reverse thrust case. After the engine cooldown period, the TMs become the sole contributor to the F_{tr} required to maintain the set 20 knots. The TM operates in motoring mode, extracting power from the FESS. A consequent steady drop in the energy is observed, down to a value of 35.4MJ in Figure 5 (a). The aircraft then decelerates to stop at the gate. As regenerative braking is used, the TMs provide the braking torque leading to a slight recovery in the stored energy.

The taxi out operation shows a similar performance. Initially the aircraft accelerates up to taxi speed, with the acceleration force leading to a high rate of FESS discharge. A steady discharge then follows during the constant velocity phase, down to a value of 18.2MJ for the idle reverse thrust case. During the engine warmup period, conditions become similar to the cooldown period leading to the flywheel charging by 4.5MJ. This includes the slight top-up during the deceleration at the take off point.

It can be seen from the middle plot that for the case of idle reverse thrust, the aircraft is able to perform the full taxi profile with 22.8MJ remaining in the flywheel, i.e., 46% of peak energy storage. This is not the case for operation with full reverse thrust, where the flywheel reaches the minimum speed limit at approximately 700s, after which further discharge is disabled. The simulation is stopped at this point and the time period 700-950s is only shown to maintain the figure scaling. The use of reverse thrust delayed the use of the maximum TM torque for flywheel charging thus reducing the time window for energy harvesting. Further simulations show that increasing the maximum TM rating to 20kNm allows operation with full reverse thrust to extract enough energy for the full taxi profile under these conditions.

5.1.2 Scenario 2 - Comparison between LO and MED Autobrake at 59 tonnes

This scenario considers use of LO and MED autobrake settings whilst keeping the reverse thrust at idle during rollout. The same engine cooldown and warmup periods as the previous scenario are considered. A more operationally practical landing weight of 59 tonnes and a take-off weight of 69 tonnes are considered. The corresponding operations are shown on Figure 7 (a) and (b). The plots are presented in the same order as for Figure (5).

An approach speed V_{land} of 134 knots is used for these cases due to the reduced weight. The aircraft speed shows a steeper gradient during rollout in Figure 7 (b) corresponding to the use of the MED autobrake setting. The first 40s of the lower plots are shown in Figure 8. For the LO setting in Figure 8 (a), the performance is similar to that in Figure 6 (a) where the TM reaches maximum torque immediately. For the MED autobrake setting, due to the limited maximum TM torque, the increased deceleration requirement is mainly obtained from the use of the mechanical brakes. The increased deceleration rate lowers the opportunity for power transfer to the flywheel. This leads to less energy storage after rollout as seen from the energy plot in Figure 7 (b), where 28.0MJ are stored with MED setting as opposed to 39.8MJ when LO setting was used, i.e. a reduction of 30%. It can be observed from the same figure that the taxi profile was completed despite the reduced initial energy capture, however the flywheel minimum energy point at 750s dropped down significantly to 7.8MJ which is very close to the flywheel protection cut-out at 5.0MJ. Further simulations showed that operation with the MED autobrake at MTOW and MLW is also possible but it will stretch the system limits even further with a minimum energy at 6.2MJ.

A comparison of Figure 7 (a) with Figure 5 (a) shows that the change in aircraft mass leads to slightly lower peak energy values in the flywheel but less overall discharge to achieve the taxi profile. The energy varies between 47.8MJ and 18.2MJ for operation at the maximum weights. The corresponding values at the practical weight of 59 tonnes are 46.6MJ and 20.6MJ, equivalent to a drop of around 3% in the peak energy storage but a gain of 13% in the remaining energy.

DOI: 10.13009/EUCASS2023-688

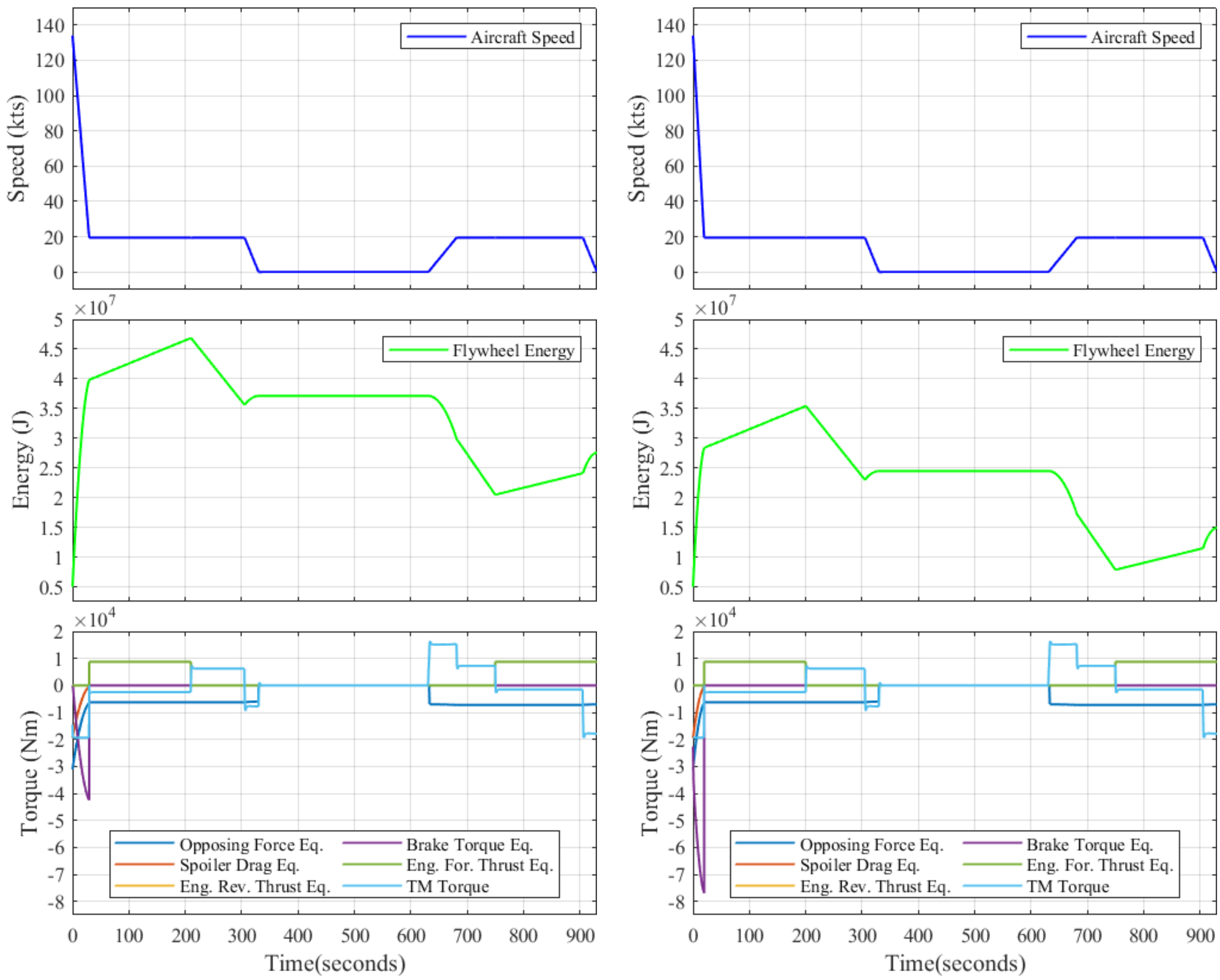

Figure 7: Aircraft Speed, Flywheel Energy and Torques for the A320 using (a) LO and (b) MED autobrake setting. Aircraft weight is 59 tonnes with idle reverse thrust setting.

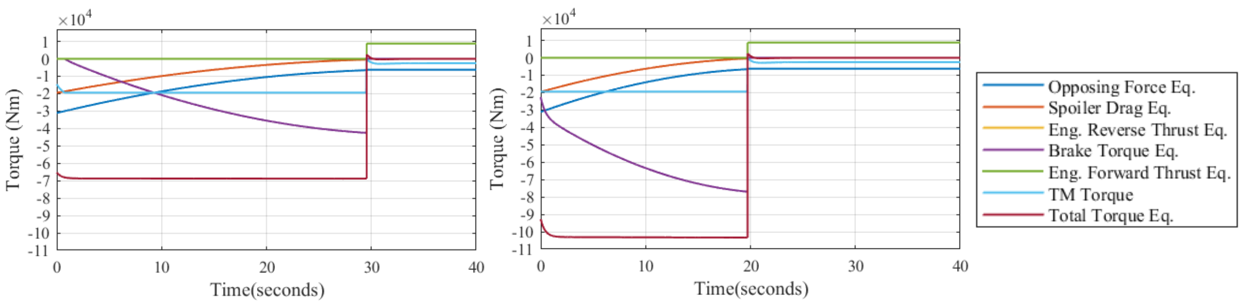

Figure 8: Deceleration torques acting during the landing roll with (a) LO and (b) MED autobrake setting. The plots correspond to the first 40s of the lower plots in Figure 7.

5.1.3 Scenario 3 – Considering a deceleration and acceleration stage in the taxi profile

In normal operations, due to ATC exigencies, the taxi profile does not usually contain one constant speed phase for taxi-in and one for the taxi-out. In order to study the effect of having to stop during a taxi phase, simulations were carried out including deceleration and acceleration events at strategic points during the taxi profile. Figure 9 (a) includes two events occurring whilst the engines are at idle while in Figure 9 (b) similar events occur whilst the engines are shutdown. MLW and MTOW were assumed in these cases in order to consider the limits of the system.

DOI: 10.13009/EUCASS2023-688

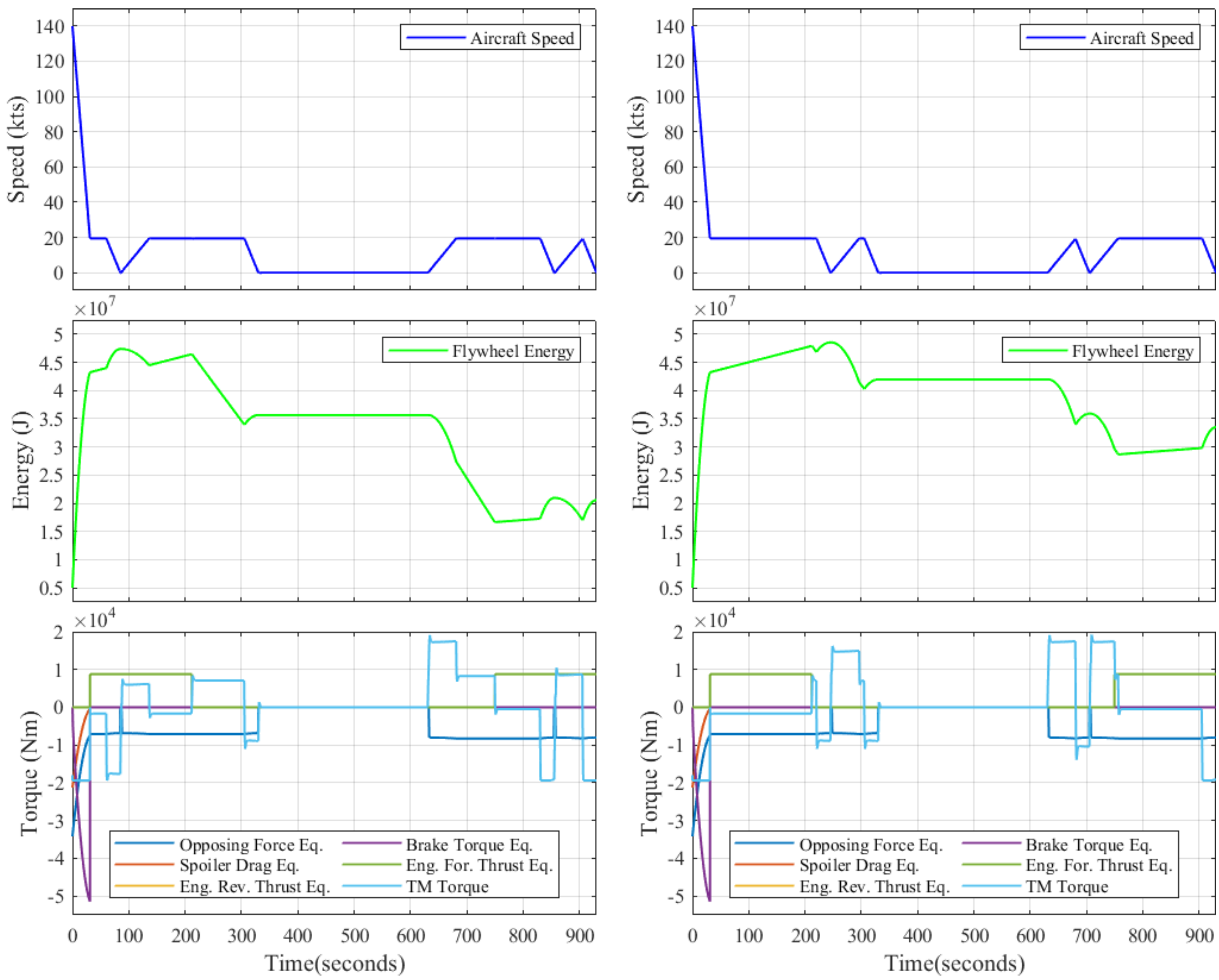

(a) (b)

Figure 9: Aircraft Speed, Flywheel Energy and Torques acting on the A320 with the introduction of deceleration/acceleration events during taxiing. Both plots consider LO autobrake and idle reverse thrust setting with a landing weight at MLW.

The deceleration and acceleration during taxi are achieved with the sole use of the TMs and no disc braking is used. When the deceleration/acceleration segment occurs during the engine idle period, as shown in Figure 9 (a), the TM torque initially has to oppose the engine thrust leading to higher energy regeneration. For the acceleration part, the torque is aided by the engine thrust thus requiring a lower value than if the engines shut down. The energy regeneration in this case is higher than the discharge leading to a slight increase in the stored energy. For the case when the deceleration/acceleration occurs during the engine shutdown period, as illustrated in Figure 9 (b), the TM torque initially goes negative to aid the opposing force F_o in braking the aircraft. During this part, power flows towards the flywheel to increase the stored energy. For the acceleration part, the TM torque reaches a higher positive value than during operation at steady speed. It is thus expected that the energy discharge during the acceleration exceeds the energy regeneration. The energy plot confirms this by showing that the energy at the end of the segment to be less than that at the beginning of the segment.

Comparison of the final energy values in the flywheel shows a different trend than the previous observation. The final energy values in the middle plots of Figure 9 (a) and (b) are 20.3MJ and 33.2MJ respectively. The corresponding value from Figure 5 (a) is of 22.8MJ, implying a decrease in the final energy values of approximately 10% and an increase of 45% for the event occurring during idle and shutdown respectively. Comparing the performances to Figure 5 (a) reveals that despite the slight net increase in energy storage in Figure 9 (a) during the deceleration/acceleration event, this is less than the steady energy rise due to the higher engine idle thrust thus leading to an overall loss of energy. For the case of Figure 9 (b), Figure 5 (a) shows a steady drop in energy during operation with the engines shut down. Despite the net drop in energy observed for the deceleration/acceleration segment when engines are shut down in Figure 9 (b), the drop is less than the steady energy drop in Figure 5 (a) leading to the higher final energy value.

DOI: 10.13009/EUCASS2023-688

5.2 ATR-72

Similar simulations were carried out for the ATR-72 model. Since the ATR-72 does not have an autobrake system, the same landing roll-out deceleration rates as for the A320 were assumed in order to have a baseline for comparison. No ground spoilers are available on the ATR and no propeller reverse pitch was taken into consideration.

5.2.1 Scenario 4 – ATR-72 with deceleration rate similar to LO at MLW

Figure 10 shows the plots for two ATR-72 cases, where part (a) presents the basic taxi profile while part (b) introduces a deceleration/acceleration event for the more restrictive case occurring whilst the engines are at idle. Both plots consider operation at the MLW of 23 tonnes (Table 1). Some differences worth noting as compared to the A320 scenarios are the initial speed of the aircraft V_{land} (113 knots), no spoiler drag, and shorter engine cooldown/warmup time of 150s. Considering Figure 10 (a), it can be observed that the engine idle thrust of the ATR-72 is also higher than what is needed in order to maintain steady speed, leading to a similar positive slope in the first and last parts of the taxi energy profile. The maximum energy reached after roll out is of 12.9MJ, which increases to 14.6MJ after cooldown, i.e., an increase of 13% which is slightly higher than for the A320. The results show that with the maximum torque of 3.3kNm per MLG, the whole taxi profile can be achieved and that similar to the A320 case study, more energy is available if the TM maximum torque is increased. The remaining energy in the flywheel at the end of the taxi period is approximately 4.8MJ, i.e., 27% of the peak energy storage. Although not presented in this paper, tests were performed for practical weights other than the MLW, and it was seen that even in the case of the ATR-72, by using the mentioned torque limits, enough energy can be harvested to achieve a full taxi profile for similar conditions to this scenario.

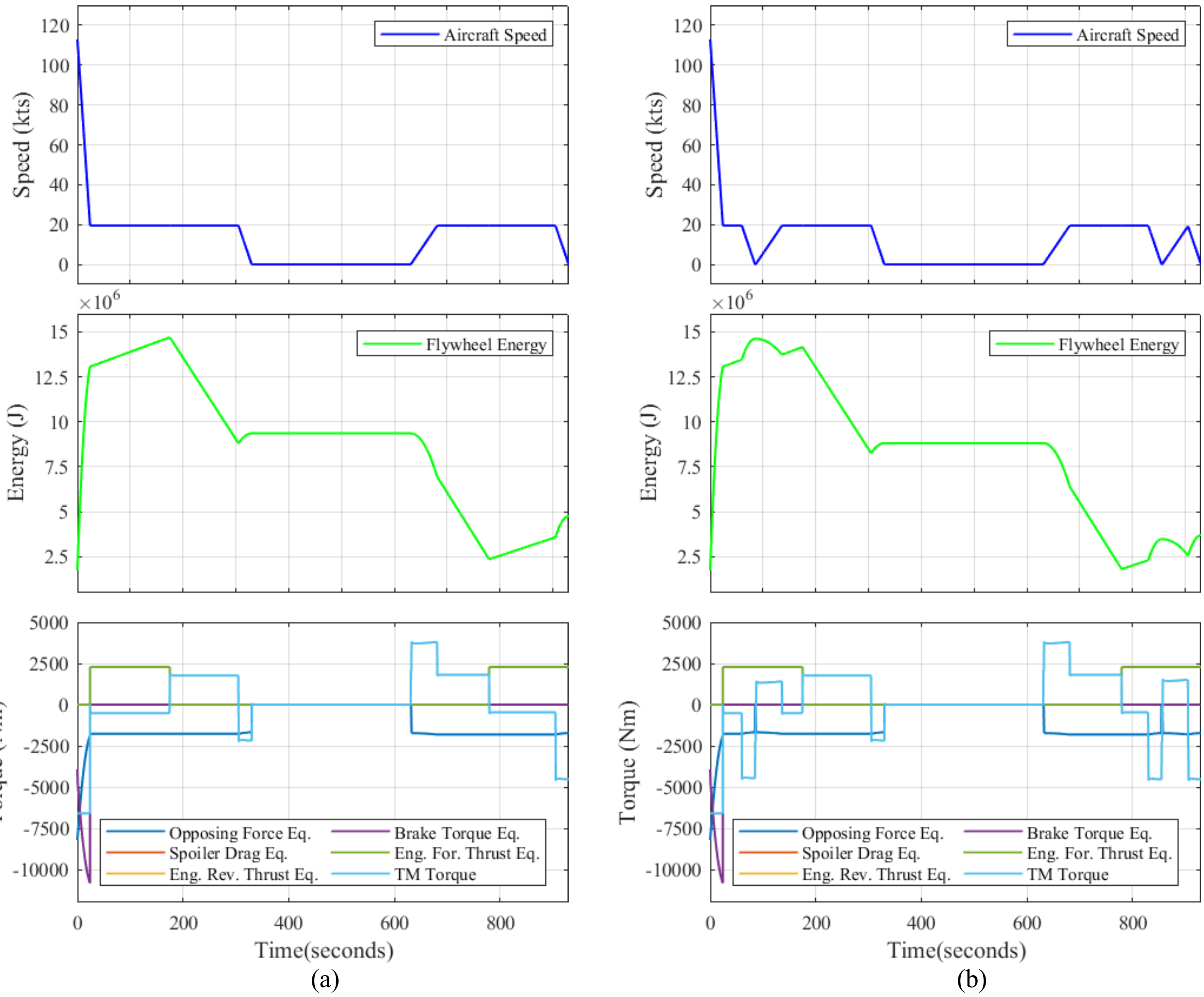

Figure 10: Aircraft Speed, Flywheel Energy and Torque acting on the ATR-72 for (a) basic taxi profile and (b) with deceleration/acceleration event. Both plots consider deceleration as for LO autobrake setting, no reverse thrust and a landing weight equal to MLW.

DOI: 10.13009/EUCASS2023-688

Figure 10 (b) shows that the performance is similar to Figure 9 (b) where a lower final energy value is observed. In this case the final energy drops from 4.8MJ to 3.7MJ, i.e., a drop of 21%. This is higher than the drop observed for the A320 case, mostly due to the higher ratio of engine idle thrust of the ATR-72 compared to the opposing forces, therefore resulting in a higher gradient for energy gain during operation with engines at idle.

6. Discussion and Conclusion

In the results section we have shown that the first three scenarios were based on the A320 and the last scenario on the ATR-72. In the first scenario, it was noted that with the use of reverse thrust during rollout, there will be less time available to harvest energy through the TMs. The reverse thrust on an A320 is dominant when compared to the other decelerating forces. When selected, it leads to a higher decelerating force than is required by the LO setting. This is not the case when the MED setting is used. The use of reverse thrust is discouraged in normal operation on a dry runway and whenever landing performance is not an issue. This is due to high fuel flow required to accelerate the engine in a very short deployment time of the reversers, noise sensitivity of the airports and engine wear. Thus, the reduced performance with full reverse thrust is not seen as a major limitation on the use of the proposed system. Whenever full reverse thrust is used, the priority would be to stop the aircraft in the landing distance available rather than on storing the energy to be used for taxi. In the first scenario, it is evident that the main limitation of the system is the short time available to extract enough energy. This can be alleviated, even in the case when using full reverse thrust, with higher TM torque ratings. The physical restrictions imposed by the mounting of the TMs on the MLG and considerations of financial viability impose maximum torque / weight restrictions. These are expected to be relaxed with the emergence of novel motor designs for aircraft electrification.

Typically, a landing aircraft does not land at MLW. Scenario 2 investigated this and used a practical mass of 59 tonnes with a lower approach speed that is appropriate for the weight. Through these tests, it was seen that the lower aircraft mass leads to slightly lower energy values in the flywheel. With this scenario, the taxi profile was managed for both scenarios although for the MED autobrake case it was stretched to its limit as the minimum energy point was close to the safety flywheel energy limit. Comparing the first two scenarios, the initial energy capture after roll-out for the full reverse thrust case was 55% less than with idle reverse, whereas the initial energy capture for the MED autobrake case was only 30% less. This means that the most stringent parameter on the system is the use of reverse thrust.

Stops during taxiing are common in everyday operation. Scenario 3 studies this reality by showing a deceleration/acceleration event during taxi. As was observed in the plots, the deceleration/acceleration segments have to displace operation with a higher discharge rate in order to leave a net energy gain effect. This was shown to happen when the segment occurs during the engine shutdown period for the considered scenarios.

Finally, scenario 4 considers the case of the ATR-72. Only a quarter of the energy harvested on the A320 is accumulated in the ATR-72 case but this energy proved to be enough to achieve the required taxi profile. The obtained energy profiles look similar with an initial increase of 11% for the A320 and 13% for the ATR-72 during cooldown. However, the remaining energy at the end of the taxi profile for the ATR-72 is lower than for the A320 at 32% instead of 46% of the peak energy value when comparing similar scenarios. This shows that the system scales accordingly and that the model remains valid for other types of aircraft.

From the results presented it is evident that during normal operation, there is sufficient energy that can be harvested from a landing aircraft that may be used for taxiing purposes. The most used setting for normal operation, with LO autobrake deceleration setting, spoilers (for the A320) and no reverse thrust, recovers enough energy to provide sufficient energy for the typical taxi time for both taxi-in and taxi-out for majority of airports. The main challenge for energy capture is the short time available during the aircraft roll out. This is limited by the safety aspect of performance limited runways or busy major airports requiring minimum runway occupancy time operation. However, this limitation can be overcome by increasing the TM torque rating.

7. Acknowledgements

Project REACTIVE is funded by the Malta Council for Science & Technology, through the SINO-Malta Fund 2020 (Science and Technology Cooperation).

DOI: 10.13009/EUCASS2023-688

References

[1] European Commission. 2011. Flightpath 2050 Europe's Vision for Aviation. European Commission, Belgium, High Level Group on Aviation Research 2011.

[2] ACI Europe. 2021 Airport Carbon Accreditation (Accessed on 15th May, 2021). [Online]. www.airportcarbonaccreditation.org

[3] Batra, A. and Camilleri R., Assessing the environmental impact of aircraft taxiing technologies, 32nd Congress of the Int. Council of the Aeronautical Sciences (ICAS2020) Shanghai, China, Sept. 7, 2021.

[4] Lukic, M., et al., 2019. Review, Challenges, and Future Developments of Electric Taxiing Systems. IEEE Trans on Transp. Electr.,(5), 4.

[5] Mahmood, T., et al., 2011. Thrust Reverser for a Separate Exhaust High Bypass Ratio Turbofan Engine and its Effect on Aircraft and Engine Performance. Proceedings of ASME Turbo Expo 2011.

[6] Eurocontrol. 2021. Taxi Times – Summer 2021 (Accessed on 17th November, 2022). [Online]. www.eurocontrol.int/publication/taxi-times-summer-2021

[7] Airbus. 2023. (Accessed on 15th June, 2023) [Online]. www.aircraft.airbus.com

[8] ATR. 2023. Avions de transport regional (Accessed on 15th June, 2023) [Online]. www.atr-aircraft.com

[9] Simple Flying. 2023. (Accessed on 19th June, 2023) [Online]. www.simpleflying.com/airbus-a320-vs-a320neo

[10] Airlines Inform. 2023. (Accessed on 24th June, 2023) [Online]. www.airlines-inform.com/commercial-aircraft/atr-72.html

[11] Airbus S.A.S., 2020. A320 Aircraft Characteristics Airport and Maintenance Planning Manual

[12] EASA. 2012. Type-Certificate Data Sheet No. EASA.A.084 for ATR 42 and ATR 72

[13] Rosenow, J., et al., 2022. Aircraft-Type-Specific Impact of Speed Brakes on Lift and Drag. MDPI Aerospace.

[14] Pmgasser.ch. 2023. (Accessed on 26th June, 2022) [Online]. www.pmgasser.ch/airbus_memos/downloads/A320_HYD.pdf

[15] Perumal, E., et al., 2022. Hybrid Power Supply for Take-off and Landing in Commercial Aircraft. International Journal for Research in Applied Science & Engineering Technology (IJRASET), Volume 10 Issue VI June 2022.

[16] Prasuhn, A. L. 1980. Fundamentals of Fluid Mechanics. Prentice Hall, Englewood Cliffs, New Jersey

[17] Sun, J., Hoekstra, J.M., and Ellerbroek, J. 2018. Aircraft Drag Polar Estimation Based on a Stochastic Hierarchical Model". Eighth SESAR Innovation Days.

[18] Grigore-Müler, O., and Barbelian, M., 2012. Regenerative braking for aircraft landing roll phase using an electric machine. Proceedings of the 13th International Conference on Optimisation of Electrical and Electronic Equipment, (OPTIM)

[19] Camilleri, R. and Batra, A., Kinetic energy recovery from a landing aircraft: Energy analysis, environmental & economic prospects, 33rd Congress of the Int. Council of the Aeronautical Sciences (ICAS2020, 4-9 Sept. 2022), Stockholm, Sweden.